Nonlinear optical transmission in multiple quantum wells with ridged waveguides: Experiment and theory

V. Pellegrini, F. Fuso, and E. Arimondo
Dipartimento di Fisica, Università di Pisa, Piazza Torricelli 2, I-56100, Pisa, Italy

F. Castelli and L. A. Lugiato
Dipartimento di Fisica, Università di Milano, Via Celoria 16, I-20123, Milano, Italy

G. P. Bava
Dipartimento di Elettronica, Politecnico di Torino, Corso Duca degli Abruzzi 24, I-10129, Torino, Italy

P. Debernardi
Centro Studi Propagazione Antenne, Consiglio Nazionale delle Ricerche, c/o Politecnico di Torino, Corso Duca degli Abruzzi 24, I-10129, Torino, Italy

(Received 4 November 1993; revised manuscript received 12 May 1994)

We report on the observations of a nonlinear optical response in the radiation pulses transmitted by a multiple-quantum-well GaAs/$Al_xGa_{1-x}As$ sample with a ridged waveguide configuration obtained by chemical etching. The nonlinear response is investigated through optical hysteresis obtained by plotting the transmitted power versus the input power. The physical conditions are complementary to those that characterize previous experiments in the field of optical bistability in multiple-quantum-well structures. The numerical simulations, obtained using the first-principles approach previously developed by some of us [G. P. Bava, F. Castelli, P. Debernardi, and L. A. Lugiato, Phys. Rev. A **45**, 5180 (1992)], are in satisfactory qualitative and semiquantitative agreement with the experimental data. The numerical simulations also prove that optical bistability could be observed in ridged waveguide samples using cw laser sources.

PACS number(s): 42.65.Pc, 78.66.−w

I. INTRODUCTION

Research on optical bistability (OB) [1–3] in semiconductors [4,5] received a noteworthy impulse from the discovery that multiple-quantum-well (MQW) structures exhibit large optical excitonic dispersive nonlinearities of the $\chi^{(3)}$ type at room temperature [6,7]. This step activated the realization and the investigation of monolithic GaAs/$Al_xGa_{1-x}As$ bistable microcavities, which are very promising for all-optical logic and signal processing (see [1,3] and references quoted therein), because, for example, they display a good thermal stability [8,9], low switching power threshold [10], a fast response time (on the order of nanoseconds) as a consequence of the fact that the nonlinearity is of electronic origin [11], and a sizable nonlinear phase shift even with samples a few micrometers wide [12].

A remarkable series of experiments in bistable MQW devices has been conducted in recent years by Oudar and collaborators [9,10,13–15]. These observations have been performed using short samples (a few micrometers in length) with efficient reflectors (reflectivity greater than 90%) to produce the high finesse required to enhance the effect of the nonlinearity and thus achieve bistability. Those MQW layers were orthogonal with respect to the direction of propagation of the radiation. Optical bistability in a InGa/As/InP MQW waveguide Fabry-Pérot cavity has been recently reported by Ehrlich *et al.* [16].

In a recent paper [17] some of us formulated a first-principles model to describe OB in MQW structures with Fabry-Pérot or distributed feedback resonators. Differently from the case of Refs. [9,10,13–15], we considered a planar waveguide configuration, with the planes of the wells parallel to the direction of propagation. The optical nonlinearities were described by means of the first-principles theory developed by Haug, Koch, Schmitt-Rink, and collaborators [18–23], generalized to include the finite width of the wells [24]. The dynamics of the system was described by the equations that govern the evolution of the two counterpropagating fields, coupled with the carrier density equation, and accompanied by the appropriate boundary conditions. The steady-state behavior was analyzed as a function of the control parameters of the system for the case of a GaAs/$Al_xGa_{1-x}As$ structure. It was shown that the system develops bistability even when the input field is in resonance with the heavy-hole exciton peak, but the phenomenon becomes more pronounced in detuned configurations.

This paper reports on the results of an experiment on OB, which was inspired by the theory of Ref. [17]. A MQW sample was chemically etched in the proper way, as described in the following section, in order to satisfy the light propagation direction suggested in the theoretical analysis. In turn, the model [17] was used to simulate the experimental observations. The characteristics of this

experiment, in several aspects, complement those of Refs. [9,10,13–15], because (i) the well system is placed in a planar waveguide configuration, i.e., parallel to the direction of propagation, and (ii) the sample is substantially longer (0.9 mm) and the mirror reflectivity is substantially smaller (~ 0.3, because there are no dielectric coatings or Bragg reflectors). The value of the absorption coefficient αL of the sample is relevant ($\simeq 0.5$), so that the single-pass effects of the interaction between radiation and the material are large, which was not the case for the parametric conditions assumed in Ref. [17]. It turns out, in the *ad hoc* numerical simulations, that also in the present configuration optical bistability is realized.

The experimental observations are concentrated on the excitation of the MQW sample through a pulsed laser source, with pulse duration comparable to the carrier recombination time. Thus the experimental observations are not able to realize an optical bistable response. Instead, an optical dynamical hysteresis response has been observed in the plots of the MQW transmitted pulse versus the incident power. Optical hysteresis itself does not have an immediate application. However, several relevant results are obtained from our investigations: (i) the observation of optical hysteresis versus laser detuning from the excitonic transitions proves that the nonlinear optical response of the MQW sample is dominated by the excitonic resonance; (ii) very good agreement between experimental observations and theoretical simulations allows a full confidence in the model.

In Sec. II we describe the experimental apparatus and the characteristics of our sample. Sections III and IV report on the results of the photoluminescence measurements and of the observations of optical hysteresis, respectively. In Sec. V we recall the first-principles model for the optical response of the material, together with a simple semiempirical model related to the photoluminescence measurements. Section VI is devoted to the description of the dynamical model, the numerical simulations, and the comparison with the experimental findings. The final Sec. VII summarizes the main results and introduces some critical considerations, also in connection with future investigations.

II. SAMPLE DESCRIPTION AND EXPERIMENT

The sample used is a GaAs/$Ga_{0.7}Al_{0.3}As$ multiple-quantum well, designated as No. 485, grown by a molecular-beam epitaxy technique using an As_4 source on a (100)-oriented GaAs semi-insulating substrate at a temperature of 600 °C [25]. The sample, grown at the CNRS laboratory in Sophia Antipolis, France, is part of a MQW batch whose photoluminescence investigation has been reported in Ref. [25]. It consists of a 0.5-μm-thick GaAs buffer layer followed by a 300-Å-thick $Ga_{0.7}Al_{0.3}As$ barrier and three identical GaAs QW's of width 79 Å embedded in 200-Å-thick $Ga_{0.7}Al_{0.3}As$ barriers.

This sample has been, furthermore, processed at the CSELT Laboratory in Torino by the photolithographic technique previously applied to InGaAsP/InP, InGaAlAs/InP samples [27]. During this processing MQW ridged waveguides have been manufactured and the GaAs substrate has been removed. The final structure of our sample is shown in Fig. 1. The distance between two consecutive MQW waveguides is 250 μm, their length is 0.9 mm, and the ridge width ranges from 6 to 50 μm; the reflection coefficient at GaAs/air interface is 0.32. The measurements presented in this paper have been performed using only the 50- and 21-μm-wide MQW ridged waveguides.

The experimental setup used in order to analyze the light transmission of a selected waveguide is shown in Fig. 2. The most relevant feature of the experimental setup is the use of single-mode optical fibers to deliver light into the waveguide and to collect the transmitted pulses after propagation through the structure in the normal direction with respect to the MQW growth axis. The single-mode optical fibers have a core diameter of 4 μm and a numerical aperture of 0.1. The pulse at the output of the second optical fiber is detected by a Hamamatsu S2381 fast photodiode (rise time <0.5 ns) connected to a Tektronix TDS540 fast digital oscilloscope; its time resolution is 1 ns on a single shot acquisition, but it can be improved up to 100 ps averaging over few tens of shots. The MQW structure and the ends of the two optical fibers are placed on the focal plane of a microscope, to control, through a charge-coupled-device camera placed on one of its two arms, the waveguide-optical fiber coupling. The laser intensity impinging on the MQW waveguide has been determined measuring the pulse energy at the end of the entrance optical fiber and dividing it by the area of the laser spot on the sample. Such a determination cannot be directly applied to the transmitted pulse, because the light is not totally transmitted by the waveguide itself but travels around it. In the experimental results the light power collected by the output fiber is reported, and we have estimated a power up to 20 mW for an input intensity up to 200 mW/μm^2.

For the optical transmission measurements the light pulse is provided by a dye laser (Lambda Physik FL2002) pumped by a XeCl excimer laser (Lambda Physik EMG101), using Styril-9 (Exciton LDS821) as dye, the tunable range of the laser being 8000–8500 Å (photon energy corresponding to 1.550–1.459 eV). The shape of the pulses is approximately Gaussian with a half width at half maximum of about 8 ns; the pulse energy is about 2 mJ at the maximum of the tuning range [8180 Å (1.516

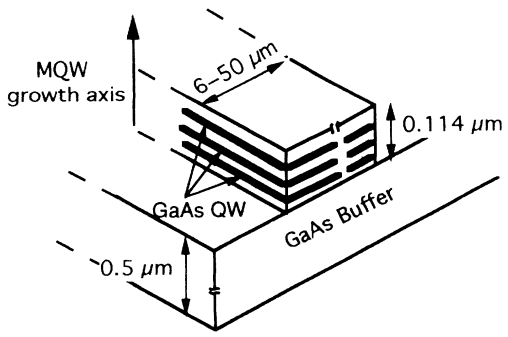

FIG. 1. Prospective view of the MQW ridged waveguide structure.

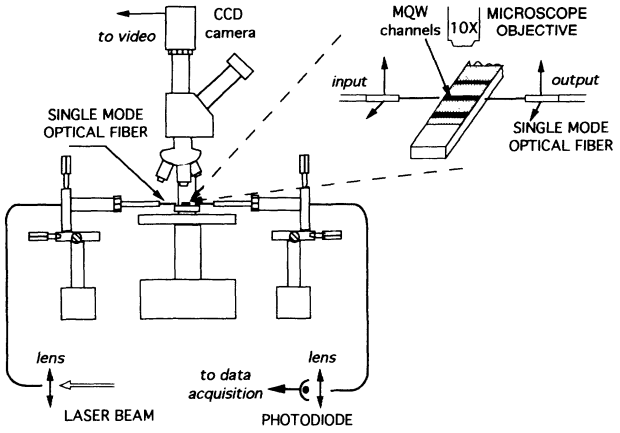

FIG. 2. Experimental setup; the inset shows the coupling between fiber ends and the MQW ridged waveguide.

eV)] for a 5-Hz repetition rate. The laser pulse has been focused and coupled to the entrance optical fiber through a 4.42-mm focal length lens; neutral density filters have been used to decrease the energy of the laser pulses. All the measurements have been performed at room temperature.

Preliminarily to the optical transmission experiment, we have also performed a study of the room-temperature photoluminescence (PL) properties of the MQW No. 485 structure previously described. Photoluminescence has been excited by a 6328-Å He-Ne laser focused, through a 50-cm focal-length lens, at an intensity of about 80 W/cm^2. Collection of the photoluminescence light has been made at 45° off normal incidence in the reflection (backward) direction through a 20-cm focal-length lens. Photoluminescence light is detected by a 64-cm Jobin-Yvon monochromator equipped with a Hamamatsu R955 phototube and lock-in amplification. Moreover, we have compared the spectra of sample No. 485 to those produced, under the same irradiation and collection conditions, by the MQW sample No. 494 with a nominally identical structure, grown under similar conditions [25] but without etched structures.

III. PHOTOLUMINESCENCE MEASUREMENTS

Before presenting the optical transmission properties of the MQW ridged waveguides, we recall its PL properties and compare its spectra with those obtained from the nonetched MWQ sample No. 494.

Figure 3 shows a typical PL spectrum of the No. 485 MQW ridged waveguide in(a) and of the standard MQW sample No. 494 in (b) under 6328-Å excitation; spectra similar to those of Fig. 3(a) have been obtained using different waveguides of the No. 485 sample. Both spectra exhibit a dominant peak due to the $n=1$ state of the heavy-hole (hh1) exciton confined in the GaAs quantum wells. In the high-energy side of the spectra there is another peak associated with the $n=1$ light-hole (lh1) exciton. However, the two spectra are very different owing to the presence of a large background in the spectrum of sample No. 494. That background has been ascribed, in previous photoluminescence studies of MQW samples, to

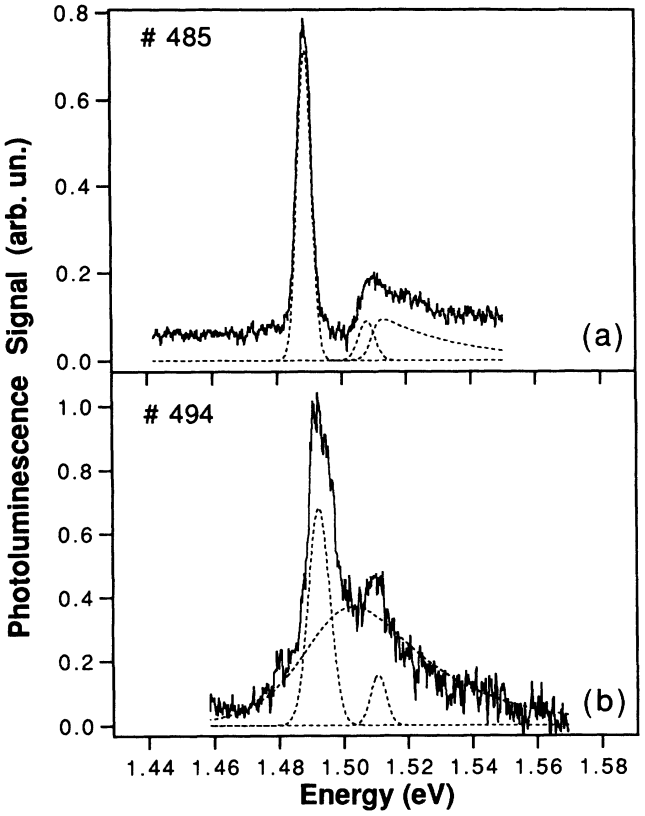

FIG. 3. Photoluminescence spectra of the No. 485 ridged waveguide MQW sample (a), and the No. 494 MQW sample with a nominally identical structure but not etched (b). The dashed lines represent the three contributions to the best fit of the line shape as obtained from a statistical analysis similar to that of Ref. [26].

free-electron-hole recombination [26], theoretically described by a broadened steplike two-dimensional density of states and a two-dimensional Sommerfeld factor [28]. We have applied a line-shape fitting procedure to heavy-hole and light-hole exciton emission and to the free-carrier recombination as performed in Ref. [26]. Those contributions, indicated by the dashed lines in Figs. 3(a) and 3(b), have relative weights and widths, in good agreement with the results of Ref. [26]. From the photoluminescence spectrum of Fig. 3(a) it appears that the free-carrier recombination is strongly reduced in the MQW sample No. 485 with ridged waveguides, the results being six times smaller than in sample No. 494.

From the line-shape fit we have determined the exciton transition energies and we have obtained, respectively, the values E_{hh1} (No. 494)=1.493 eV, E_{lh1} (No. 494)=1.511 eV, E_{hh1} (No. 485)=1.489 eV, and E_{lh1} (No. 485)=1.508 eV, in good agreement with the known dependence of the heavy- and light-hole resonances with the temperature and the quantum-well dimensions [26,29]. The observed energy differences should actually reflect the slight differences in the growth conditions of the two samples or possible fluctuations in the exact determination of the nominal thickness of the GaAs quantum wells.

The drastic change in the background electron-hole recombination in sample No. 485 can only be ascribed to its ridged waveguide structure. A possible consequence of the presence of this structure is an alteration of the free-carrier diffusion processes and of the consequent recombination processes. It may be supposed that the recombination takes place through diffusion to the ridge walls and nonradiative processes produced by impurities or irregularities on the walls.

IV. OPTICAL TRANSMISSION MEASUREMENTS

In this section we will present the results of the investigation on the nonlinear response of the No. 485 MQW ridged waveguide excited according to the setup described in Sec. II. It will be shown that the MQW nonlinear optical response produces a drastic modification of the light pulse transmitted by the sample. This modification appears as a dynamical optical hysteresis when the transmitted light intensity is plotted versus the incident intensity. Special emphasis will be given to the analysis of the width of such an optical hysteresis loop as a function of the incident pulse photon energy and of the laser frequency on or off resonance with one of two excitonic transitions (hh1 or lh1). The dependence of the hysteresis loop area allows the enlightenment of the role of nonlinear absorptive and dispersive response, which would determine the observation of optical bistability under a cw laser excitation.

When the MQW ridged waveguide sample is excited by the pulsed dye laser light near resonance with the excitonic transitions, the pulse transmitted through the sample is strongly attenuated. Moreover, the incident Gaussian shape is heavily distorted, and superimposed oscillations are present on the transmitted pulse. In order to represent clearly those modifications associated to the nonlinear response of the MQW waveguide, Fig. 4 reports the transmitted power P_T versus the incident intensity I_I, as derived from the pulse time dependences, for various laser photon energies at the maximum achievable excitation intensity; the time resolution is 1 ns and the acquisition is made over one single laser shot. For incident intensity we use the pulse detected at the end of the output single-mode optical fiber without propagation through the MQW waveguide; in this way, we take care of possible distortions caused by the passage through the optical fibers system.

As clearly shown, large hysteresis loops are observed, except for the cases where the laser pulse is quasiresonant with the hh1 [Fig. 4(b)] and lh1 [Fig. 4(e)] excitonic transitions. Except for these two cases, the direction of all the hysteresis loops is counterclockwise, while the direction of the residual loops of Figs. 4(b) and 4(e) is clockwise. Note that the largest hysteresis loop is observed when the excitation photon energy is in between the energy of the two excitonic transitions [Fig. 4(c)], suggesting that the simultaneous dispersive contribution of the two excitonic resonances enhances the nonlinear behavior. In order to demonstrate that the modifications in the light transmitted by the MQW sample are created by the non-

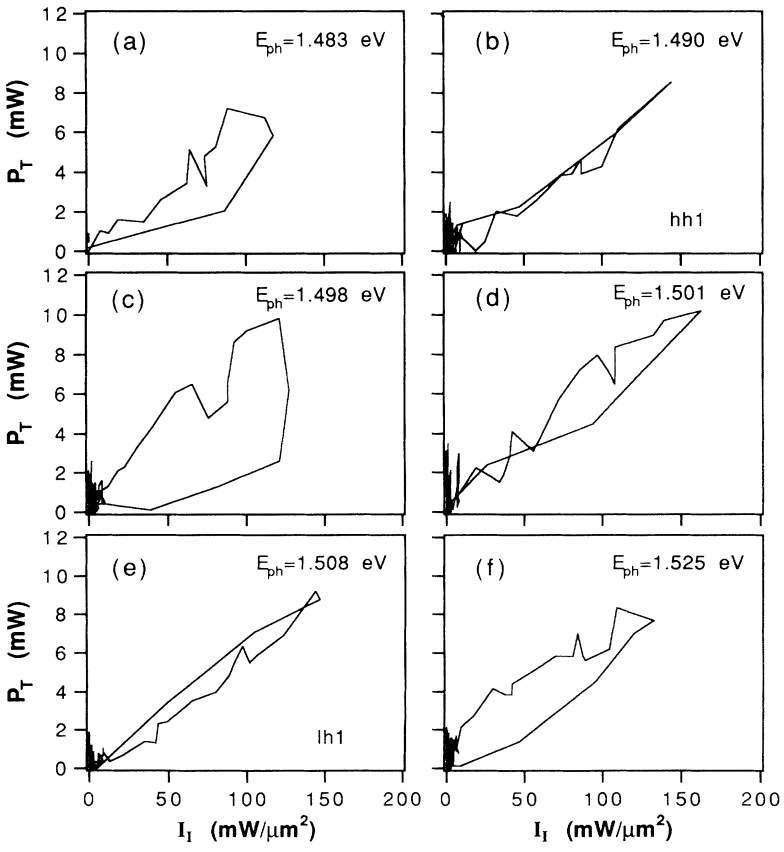

FIG. 4. Transmitted power P_T vs incident intensity I_I for various incident laser photon energies (indicated on the graphs). Graph (b) and graph (e) correspond to resonant excitations with respect to the heavy-hole (hh1) and light-hole (lh1) exciton transitions, respectively.

linear optical response of the excitonic resonances, Fig. 5 reports the area of the observed optical hysteresis loop versus the laser photon energy, at a fixed value of the incident laser intensity (maximum intensity of the optical pulse $I_M = 120$ mW/μm^2). It may be observed that for the laser quasiresonant with the hh1 and lh1 transitions, the area of the hysteresis loop is small and negative, i.e., with an evolution of the cycle in the clockwise direction. The maximum of the counterclockwise hysteresis loop is observed in conditions of dispersive nonlinear response.

Another important point of our analysis is the determination of the intensity threshold above which we can observe hysteresis behavior. For this purpose at fixed excitation photon energy, we have changed the incident intensity using neutral density filters, in the range 0.2–200 mW/μm^2. We have chosen the photon energy $E_{ph} = 1.498$ eV, corresponding to Fig. 4(c), because of the large hysteresis loop observed in the measurements reported above. The results of such an analysis are presented in Fig. 6, where the time resolution is 100 ps and the signal is averaged over 100 laser pulses. The shape of the hysteresis loop obtained at the maximum intensity [Fig. 6(a)] is qualitatively similar to that of the correspondent hysteresis loop of Fig. 4(b). The amplitude of the hysteresis loop is reduced, decreasing the input intensity and curves (b) and (c). We estimate the appearance of a hysteresis loop when the incident intensity is larger than $I_I = 1.5 \pm 0.3$ mW/μm^2. At an intensity of 0.35 mW/μm^2 [Fig. 6(c)] the MQW response is linear. The direction of all the obtained loops is counterclockwise, as in Fig. 4(c).

Threshold values for the excitonic-type bistable behavior appearance in MQW obtained in previous works [14,30] have been estimated in a few tens of μW/μm^2, but in these cases the MQW structure was inserted in a cavity with a reflection coefficient $R \approx 0.9$, as already pointed out in the Introduction. In our case, we exploit only the interface GaAs/air ($R = 0.32$) without using any further cavity; this reduction in reflectivity leads to a higher threshold intensity, as observed in our measurements.

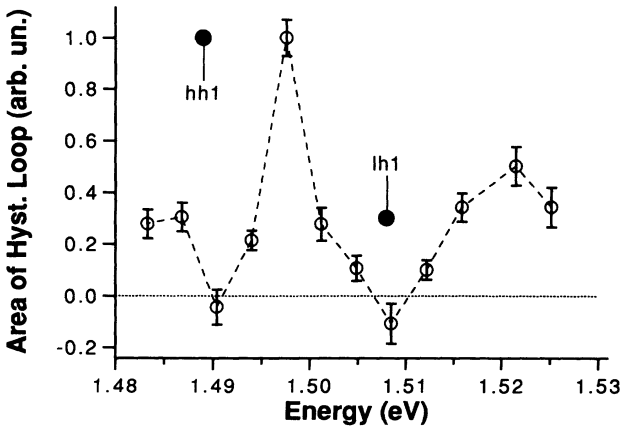

FIG. 5. Area of the hysteresis loop vs incident photon energy; the maximum intensity of the optical pulse is $I_M = 120$ mW/μm^2. Also shown in the graph are the positions of the excitonic transitions hh1 and lh1 (black circles) as given by the photoluminescence spectrum of Fig. 3(a).

V. MODEL OF THE NONLINEAR OPTICAL RESPONSE

A. First-principles model

A consistent model of the nonlinear dielectric response in MQW structures must include a combination of many-body effects such as the Coulombic interaction between carriers and the exclusion principle [22]. At room temperature, the most important effects are represented by the renormalization of the band gap and the screening of the Coulomb interaction by increasing carrier density. As a consequence, the optical nonlinearity is directly related to the carrier density generated by the optical absorption. Assuming transients slow with respect to the intraband relaxation times, the carrier energy distributions are represented by the Fermi-Dirac statistics.

The model accounts for one conduction and two valence subbands (the first heavy and light hole), and it includes correctly the effects of the finite well thickness. The contribution $\Delta\varepsilon$ to the dielectric constant, due to the interaction of the electromagnetic field at the angular fre-

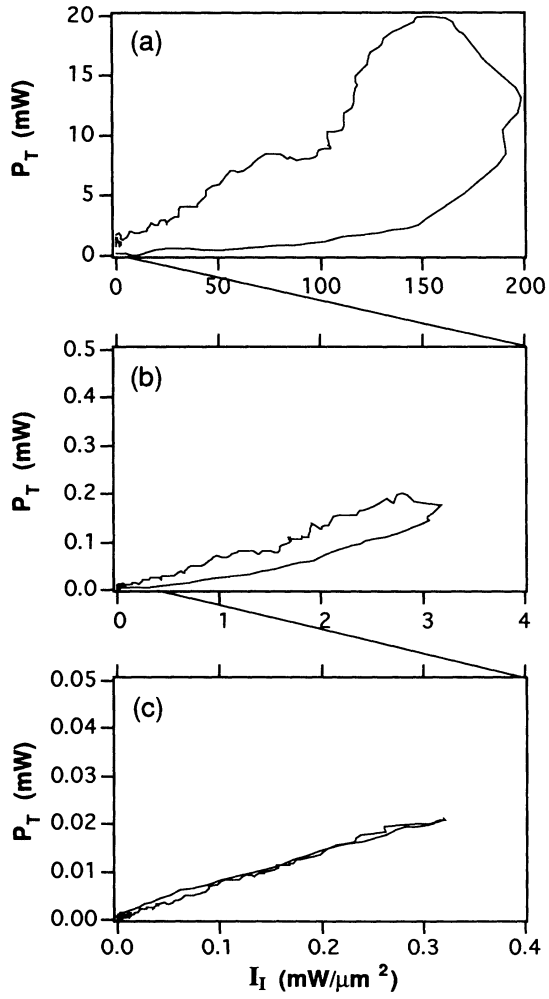

FIG. 6. Transmitted power P_T vs incident intensity I_I loops as a function of the incident intensity progressively reduced from (a) to (c). Notice the expansion of the horizontal scale in these diagrams. Laser photon energy is $E_{ph} = 1.498$ eV, between the two exciton transitions.

quency ω with the carrier density per unit area N in a well of thickness d, is given by the sum of the contributions from the heavy-conduction and light-conduction transitions, and is written as

$$\Delta\varepsilon(\omega,N)=\frac{2}{V}\sum_{\mathbf{k},n}\mu_{k,n}\chi_{k,n} , \tag{1}$$

where V is the volume of the well ($=Ad$, with A reference area), $\mathbf{k}$ is the particle wave vector parallel to the QW layer, $\mu_{k,n}$ denotes the dipole matrix element between conduction and valence band at a given wave vector $\mathbf{k}$ and for TE polarization. The microscopic polarizations $\chi_{k,n}$ satisfy a set of two coupled integral equations of the Bethe-Salpeter type [31].

The finite well thickness influences in a substantial way the matrix elements of the potentials, which appear explicitly in the Bethe-Salpeter equations. For instance, regarding the electron-hole potentials, they can be expressed in terms of the quantities

$$V_{\mathrm{eh}}(k,k',q)=V_{\mathrm{2D}}\int_{z_1}\int_{z_2}|\Phi^{C}(z_1)|^2\Phi^{A*}(z_2,k)\Phi^{B}(z_2,k') \times e^{-q|z_1-z_2|}dz_1dz_2 , \tag{2}$$

where Φ are the electron and hole normalized wave functions in the potential well, C indicates a conduction sub-band, A and B refer to the two possible spin configurations of a valence sub-band, the k dependence of the hole wave functions accounts for valence-band mixing, and $q=|k'-k|$. Similar expressions hold for the electron-electron and hole-hole interactions. In the limit case where the well thickness $d\to 0$ and the potential well $\to\infty$, the preceding expression reduces to the more familiar two-dimensional (2D) potential $V_{\mathrm{2D}}(q)=e^2/2qA\varepsilon$, where ε is the bulk dielectric constant.

The band-gap renormalization, which arises from the electron-hole plasma, is determined as [17,18]

$$\Delta E_g=\sum_q\{\tfrac{1}{2}[V_{s,\mathrm{ee}}-V_{\mathrm{ee}}]+\tfrac{1}{2}[V_{s,\mathrm{hh}}-V_{\mathrm{hh}}] -[V_{s,\mathrm{ee}}f_{eq}+V_{s,\mathrm{hh}}f_{hq}]\} , \tag{3}$$

where the various quantities V are computed with expressions similar to Eq. (2) and the suffix s means that the screening is included by a static, single-plasmon pole approximation. In the preceding equation, the f_q are the electron and hole distribution functions; in this model, ΔE_g depends on the well thickness d through the Coulomb potential.

The well thickness plays a very important role in the nonlinear optical response; on the one hand, too small values of d give rise to a vanishing contribution to the MQW effect due to both the spreading of the wave functions and the decreasing value of the overlap integral with the electric field of the guided mode; on the other hand, by increasing d the behavior approaches the bulk characteristics with a reduced excitonic interaction.

Equation (3) is solved by approximating the sum with an integral and by solving the resulting integral equation. The numerical solution of the Bethe-Salpeter integral equation system discretizes the unknown functions and solves the corresponding set of linear algebraic equations for the unknown values.

For a GaAs/Al_xGa_{1-x}As QW structure, using the numerical values for the material parameters given in [31], the absorption (related to $\mathrm{Im}\{\Delta\varepsilon/\varepsilon\}$) and the refractive index (related to $\mathrm{Re}\{\Delta\varepsilon/\varepsilon\}$) are shown in Fig. 7, with the carrier density N (normalized with respect to the square of the two-dimensional Bohr radius a^2) as a parameter. In particular, in Fig. 7(a), the exciton resonance peaks (hh1 and lh1) and their quenching by increasing carrier density are well evident.

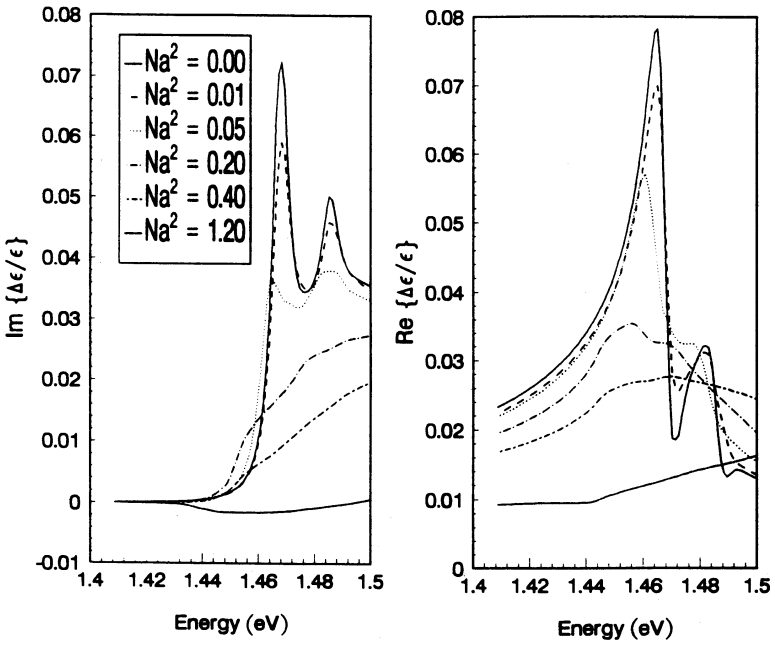

FIG. 7. Imaginary (left) and real (right) part of the dielectric constant vs excitation photon energy spectra for a 79-Å GaAs/Al_xGa_{1-x}As QW by varying carrier density normalized to the 2D Bohr radius $a=62$ Å.

B. Semiempirical model

The results of Sec. V A, compared with the experimental photoluminescence measurements of sample No. 485 [Fig. 3(a)], show a certain difference, mainly in the valley between the two excitonic resonances. In particular, the photoluminescence curves show a stronger minimum and a less relevant influence of the band-to-band transitions. This different behavior is not completely clear, but it could be attributed to the ridged structure of the sample, as we discussed at the end of Sec. III.

In order to achieve a better agreement between the material model and such experimental data, only the two excitonic resonances have been considered for an empirical model of the optical response, by assuming proper Lorentzian shapes [32]; in particular, the contribution of the single well to the dielectric constant $\Delta\varepsilon$ is written as a sum of the parts of the heavy-hole (hh) and light-hole (lh) exciton:

$$\frac{\Delta\varepsilon}{\varepsilon}=g(n)\sum_{j=\mathrm{hh,lh}}M_j\frac{1}{\Theta_j(n)-i}\ , \tag{4}$$

where M_j is the height of the excitonic peaks, $\Theta_j(n)$ is the detuning between the central frequency of the exciton peak $E_j(n)/\hbar$ and the working frequency ω, and it is expressed by

$$\Theta_j(n)=\frac{E_j(n)/\hbar-\omega}{\gamma_j}\ , \tag{5}$$

where γ_j is the linewidth of the excitonic resonance, $E_j(n)=E_{g2D}-E_{j0}(1+bn^c)$, with E_{g2D} being the two-dimensional energy gap, and E_{j0}, the exciton energy at zero normalized carrier density $n=Na^2$. The density-dependent term bn^c (b and c being proper numerical constants) is introduced to account for the shift of the excitonic frequency due to renormalization of the band gap [18]. Finally, $g(n)$ describes saturation of the two excitonic peaks by increasing carrier density, and usually is given as a polynomial approximation [in our case, we can take $g(n)=1-n/n_s$, n_s being the saturation value [32]].

By properly choosing the values of the various parameters of this Lorentzian description, it is possible to reproduce quite well the optical response calculated with the first-principles model, with exclusion of the contribution due to band-to-band transitions related to unbounded states, thus obtaining a better simulation of the experimental photoluminescence spectra shown in Fig. 3(a). An example of the quantities $[\mathrm{Im}\{\Delta\varepsilon/\varepsilon\}]$ and $[\mathrm{Re}\{\Delta\varepsilon/\varepsilon\}]$, which are utilized for the numerical simulations of the experiment as described in the next section, are shown in Fig. 8 for some values of the normalized carrier density n, as a function of the relative normalized detuning (a useful parameter for numerical simulations):

$$\Delta=\frac{\hbar\omega-E_{g2D}}{E_x} \tag{6}$$

between the photon energy $\hbar\omega$ and the two-dimensional band gap, where E_x is the two-dimensional heavy-hole exciton binding energy. The bleaching of the excitonic resonance peaks by increasing carrier density (which can grow up to a value $n_s\simeq 0.2$) is very evident again.

VI. NUMERICAL SIMULATION OF THE EXPERIMENT

A. Dynamical model for the nonlinear interaction

The nonlinearity in the field-carrier interaction will be introduced through coupled-mode theory [33], but con-

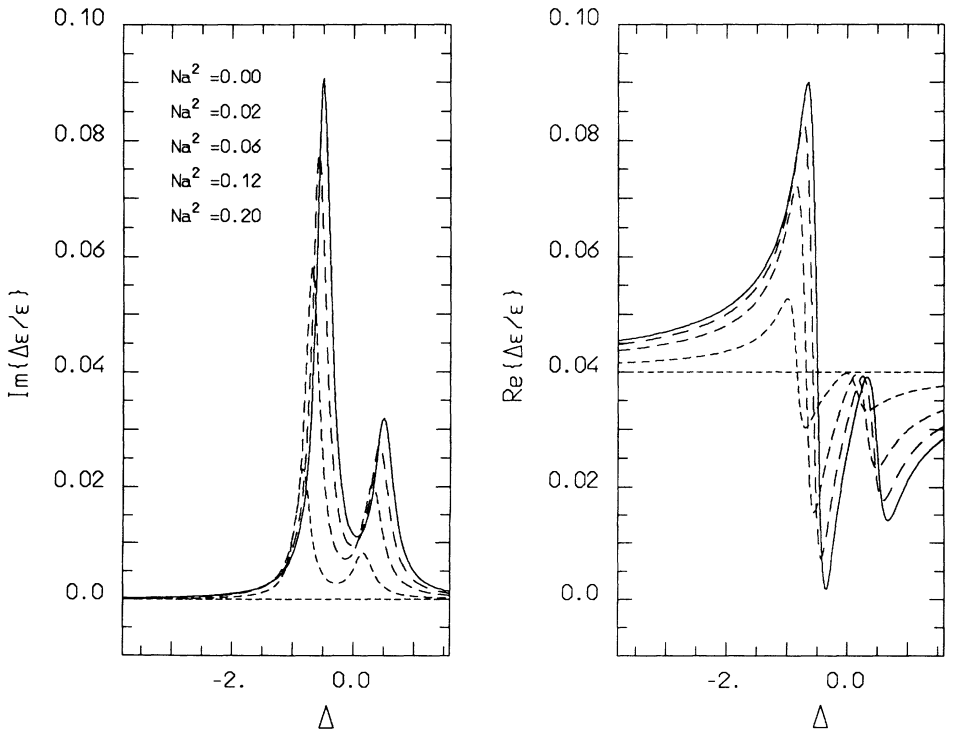

FIG. 8. Imaginary (left) and real (right) part of the dielectric constant vs excitation photon energy spectra for the same material as in Fig. 6, calculated with the semiempirical Lorentzian model, as a function of the normalized detuning Δ.

sidering strongly predominant only a single transverse mode (in our case the TE_{00}) of the optical waveguide interested by the incident laser pulse. In practical situations, this assumption is rather satisfactory since the coupling to other modes is very small and, moreover, we can suppose that the waveguide is working in monomodal conditions. In the framework of the coupled-mode approach, if $C_F(z,t)$ and $C_B(z,t)$ denote the slowly varying (in the longitudinal direction z and in time) amplitudes of the forward and backward traveling waves, respectively (normalized so that their squared moduli correspond to the traveling power per unit guide width), the following equations hold [3,17,33]:

$$\frac{\partial C_F}{\partial z}+\frac{1}{v_g}\frac{\partial C_F}{\partial t}=+\left[\frac{i\omega m\eta}{2v_g}\frac{\Delta\varepsilon}{\varepsilon}-\alpha_i\right]C_F\ , \tag{7a}$$

$$\frac{\partial C_B}{\partial z}-\frac{1}{v_g}\frac{\partial C_B}{\partial t}=-\left[\frac{i\omega m\eta}{2v_g}\frac{\Delta\varepsilon}{\varepsilon}-\alpha_i\right]C_B\ , \tag{7b}$$

where v_g is the mode group velocity, α_i is the mode attenuation due to the material intrinsic losses (excluding the interaction with the carriers), m represents the number of wells of thickness d, and η is a filling factor which takes care of the structure of the mode field distribution in the waveguide and measures the amount of optical power in a well with respect to the total mode power. Notice that in the derivation of these equations a spatial average over the transverse variables was included, in order to consider the dielectric function $\Delta\varepsilon$ as it was only dependent on the working frequency ω and the local normalized carrier density $n(z,t)$.

Equations (7a) and (7b) must be coupled with the evolution equation for $n(z,t)$, so we introduce the rate equation for the carriers in a well [17,32]:

$$\frac{\partial n}{\partial t}=-R(n)+\frac{\eta a_0^2}{\hbar v_g}\mathrm{Im}\left\{\frac{\Delta\varepsilon(n)}{\varepsilon}\right\}(|C_F|^2+|C_B|^2)\ , \tag{8}$$

where

$$R(n)=An+Bn^2 \tag{9}$$

accounts for the recombinations (typical values in GaAs for the coefficients are $A=0.2\times10^9\ \mathrm{s}^{-1}$ and $B=5\times10^{-4}/a^2\ \mathrm{s}^{-1}$). The second term on the right-hand side of Eq. (8) describes optical carrier generation due to the "local optical power" $P_l=|C_F|^2+|C_B|^2$; more rigorously, one should include the carrier diffusion effects along z and also the spatial grating due to the beat of forward and backward waves; for simplicity, it has been assumed that diffusion compensates for such a grating, since the diffusion length is larger than the grating period.

Equations (7a), (7b), and (8) include all the dynamical aspects of the interaction between fields and carrier density, and they must be completed with the boundary conditions of the Fabry-Pérot (FP) -type resonator constituted by the MQW waveguide; these boundary conditions can be written [3,2]

$$\begin{aligned}
&C_F(0)=\sqrt{T}\,C_i+\sqrt{R}\,C_B(0)\ ,\\
&C_B(L)=\sqrt{R}\ e^{-i\delta}C_F(L)\ ,\\
&C_r=\sqrt{R}\,C_i-\sqrt{T}\,C_B(0)\ ,\\
&C_t=\sqrt{T}\,C_F(L)\ ,
\end{aligned} \tag{10}$$

where C_i, C_r, and C_t are the incident, reflected, and transmitted amplitudes outside the resonator, respectively; T and R are the transmission and reflection coefficients of the GaAs/air interface (with $T+R=1$) and $\delta=(\omega_c-\omega)2L/v_g$ is the cavity detuning parameter, with L being the length of the waveguide, while ω_c is the longitudinal cavity frequency (evaluated using the unperturbed effective refractive index) nearest the input field frequency ω.

The model equations for the field-carrier interaction in a FP resonator are now complete; in this formulation they can describe static solutions, as shown in Ref. [17], or, more generally, the dynamical behavior induced by injecting an optical pulse in the MQW waveguide, as in our experiment. In the first case, we consider a constant incident power $|C_i|^2$ and, by dropping the derivatives with respect to time in Eqs. (7a), (7b), and (8), we have a set of ordinary differential equations in the longitudinal variable z, which can be solved numerically with an iterative technique [17]. We obtain the incident power $|C_i|^2$ as a single-valued function of the transmitted power $|C_t|^2$; inverting this relation, we have the static transmission characteristics of the nonlinear device, where bistable behavior appears as an S-shaped curve in the plot of output power versus the input intensity, as discussed in Sec. VI B.

In the second case, the incident power $|C_i|^2$ is a known function of time, and consequently the transmitted and reflected powers ($|C_t|^2$ and $|C_r|^2$) also are functions of time, which must be calculated solving the full system of partial differential equations (7a), (7b), and (8), with the boundary conditions (10). This can be done using a finite-difference method, like the well-known Risken-Nummedal algorithm [34]; however, this method is very computer time consuming because an accurate description of the huge length of the MQW sample requires a division of the spatiotemporal grid over some hundreds of points.

It is possible, however, to reduce the complexity of the problem using the adiabatic elimination principle [35]. As a matter of fact, the time scales of evolution for the fields and the carrier density are completely different: we will see that the ratio of the time derivatives is larger than 10^5, mainly as a consequence of the slow recombination rate of the carriers. Hence the fast field variables C_F and C_B can be eliminated adiabatically. To obtain a simplified set of equations by using the adiabatic elimination, it is useful to consider normalized forward and backward fields, together with normalized incident, transmitted, and reflected amplitude ($\mathcal{N}$ being the normalization constant),

$$\begin{aligned}
&F_F=\mathcal{N}C_F,\quad F_B=\mathcal{N}C_B,\quad Y=\mathcal{N}/\sqrt{T}\,C_i\ ,\\
&X=\mathcal{N}/\sqrt{T}\,C_t,\quad F_r=\mathcal{N}/\sqrt{T}\,C_r,\quad \mathcal{N}=\sqrt{a_0^2\eta/\hbar v_g A}\ ,
\end{aligned} \tag{11}$$

and normalized time and space variables

$$\tau = At, \quad \bar{z} = \frac{\omega m \eta}{2 v_g} z \ , \tag{12}$$

so that Eqs. (7a), (7b), and (8) can now be written

$$\frac{1}{\gamma}\frac{\partial F_F}{\partial \tau} = -\frac{\partial F_F}{\partial \bar{z}} + \left[i\frac{\Delta\varepsilon}{\varepsilon} - \bar{\alpha} \right] F_F \ , \tag{13a}$$

$$\frac{1}{\gamma}\frac{\partial F_B}{\partial \tau} = +\frac{\partial F_B}{\partial \bar{z}} + \left[i\frac{\Delta\varepsilon}{\varepsilon} - \bar{\alpha} \right] F_B \ , \tag{13b}$$

$$\frac{\partial n}{\partial \tau} = \mathrm{Im}\left\{ \frac{\Delta\varepsilon(n)}{\varepsilon} \right\} (|F_F|^2 + |F_B|^2) - n - \xi n^2 \ , \tag{13c}$$

where $\bar{\alpha} = \alpha_i \times 2 v_g / (\omega m \eta)$, $\xi = B/(Aa_0^2)$, and $\gamma = \omega m \eta / 2A$ has typically a value larger than 10^5 for practical MQW waveguide parameters (in our case, $m = 3$ and $\eta = 0.0695$).

It is clear that the left side of the two field equations is very small with respect to the left side of the carrier equation, and we can neglect them (i.e., we set the time derivative equal to zero); in this way we obtain a pair of simple differential equations for the forward and backward fields, which can be immediately integrated, obtaining

$$F_F(\bar{z},\tau) = F_F(0,\tau) \exp\left[-\bar{\alpha}\bar{z} + i\int_0^{\bar{z}} dx \frac{\Delta\varepsilon}{\varepsilon}(x,\tau) \right] , \tag{14a}$$

$$F_B(\bar{z},\tau) = F_B(0,\tau) \exp\left[+\bar{\alpha}\bar{z} - i\int_0^{\bar{z}} dx \frac{\Delta\varepsilon}{\varepsilon}(x,\tau) \right] , \tag{14b}$$

from which it is clear that the spatiotemporal evolution of the fields strictly depends on $\Delta\varepsilon$, which is a function of the carrier density $n(\bar{z},\tau)$.

Taking into account these expressions with the boundary conditions (10) and the rescaling (11), it is rather easy to obtain the following expressions for the transmitted and reflected fields, respectively, as a function of the dielectric function $\Delta\varepsilon$:

$$X(\tau) = F_F(0,\tau) \exp\left[-\bar{\alpha}L + i\int_0^L dx \frac{\Delta\varepsilon}{\varepsilon}(x,\tau) \right] , \tag{15a}$$

$$F_r(\tau) = \sqrt{R}\, Y(\tau) - F_B(0,\tau) \ , \tag{15b}$$

with

$$F_F(0,\tau) = TY(\tau) \times \left[1 + \frac{R}{\exp\left[2\bar{\alpha}L + i\delta - 2i\int_0^L dx\, \Delta\varepsilon/\varepsilon \right] - R} \right] , \tag{16a}$$

$$F_B(0,\tau) = \frac{T\sqrt{R}\, Y(\tau)}{\exp\left[2\bar{\alpha}L + i\delta - 2i\int_0^L dx\, \Delta\varepsilon/\varepsilon \right] - R} \ . \tag{16b}$$

In this formulation, the complex spatiotemporal evolution is decoupled; the temporal variable is only present in the equation for the density of carriers (13c), which depends parametrically on the spatial coordinate z. After insertion of Eqs. (14a) and (14b) into Eq. (13c), we have

$$\frac{\partial n}{\partial \tau} = \mathrm{Im}\left[\frac{\Delta\varepsilon}{\varepsilon} \right] \left\{ e^{-2\bar{\alpha}\bar{z}} \left| F_F(0,\tau) \exp\left[i\int_0^{\bar{z}} dx\, \Delta\varepsilon/\varepsilon \right] \right|^2 + \exp(+2\bar{\alpha}\bar{z}) \left| F_B(0,\tau) \exp\left[-i\int_0^{\bar{z}} dx\, \Delta\varepsilon/\varepsilon \right] \right|^2 \right\} - n - \xi n^2 \ . \tag{17}$$

From this final equation for the carrier density it appears that the strategy for the solution of the nonlinear system is the following, based on three principal steps: (i) after discretizing the length of the MQW sample into a proper number of spatial points $\bar{z}_i$, the boundary values for the fields at each time are calculated using Eqs. (16a) and (16b) by solving the integral with the trapezoidal rule; (ii) the time evolution of n is calculated from Eq. (17) with a second-order Euler method for each spatial point $\bar{z}_i$; (iii) the obtained values of n are used to calculate the optical response $\Delta\varepsilon$, using the complete model or the semiempirical model described in Sec. V. This procedure is repeated cyclically again and again. With this algorithm it is possible to simulate quite accurately our experiment, introducing the appropriate temporal shape for the incident amplitude Y and the geometrical factors to relate the optical power supplied by the optical fiber to the power effectively injected in the MQW waveguide.

B. Numerical results

In this section we will present the numerical simulations of our experiment, obtained with the dynamical model previously described, comparing at the same time with the calculated static response of the device. The experimental observations, for instance, the dynamical hysteresis cycles and their modifications as a function of the control parameters, are well reproduced, at least qualitatively; as a matter of fact, a full quantitative description of the experiment can only be obtained after an accurate analysis of the losses of the laser optical power in the experimental setup. For example, we must consider the fraction of power carried by the input fiber injected into the interaction region of the MQW waveguide, the fraction of power collected by the output fiber, the misalignment of the fibers, and so on. Such complete analysis presents considerable difficulties and it is beyond the scope of this paper.

To best match quantitatively the numerical results with the corresponding experimental curves, we have introduced two additional adjustable filling factors: the first is a measure of the fraction of optical power injected into the waveguide; the second plays the same role for the output power (typical values are 0.01 or less). Furthermore, the output optical power is increased by a small fraction of the input power (not injected in the MQW

waveguide), because there is the possibility of a direct passage of the optical power between the two fibers, due to small misalignment of the apparatus. These empirical factors are adjusted and kept fixed for each group of experimental tests, and they do not affect the computer algorithm for the solution of the dynamical model, which is almost totally independent of control parameters or geometrical factors. In particular, the following numerical simulations are expressed as a function of the normalized detuning Δ [defined in Eq. (6)], which allows us to easily identify the position of the incident photon energy of the laser beam with respect to the two exciton peaks, as shown in Figs. 7 and 8.

Some examples of dynamical optical hysteresis loops calculated from our equations, under the same conditions of the experiment and using the semiempirical model for the optical response (Sec. V B), are shown in the following figures; we plot the transmitted power $P_T=|C_t|^2 w$ versus the incident intensity $I_I=|C_i|^2/h$, w and h being the width of the output fiber and the height of the MQW waveguide, respectively; both quantities are properly corrected with the previously discussed filling factors. In all the figures the convention, by which the full line represents the dynamical hysteresis loop obtained with a variable optical signal and the dashed line is the static response of the sample, is adopted.

In Fig. 9 we have assumed $\delta=0$, i.e., resonance with a cavity mode, and we have varied the position of the laser photon energy under the exciton peaks as indicated in each diagram; the optical signal injected was a Gaussian shaped pulse with half width at half maximum of 8 ns and a peak power intensity of 180 mW/μm^2, as in the experiment. All the hysteresis cycles were covered counterclockwise.

It is well evident that static bistability (or more precisely multistability, as the curves have more than a region with negative slope) is only present when the laser photon energy is far from resonance with the exciton peaks [Figs. 9(a) and 9(f)], while in the other cases the curves are nearly linear (piecewise). On the contrary, the dynamical hysteresis loop is observed in all the cases, as a consequence of the delayed dynamics [36] of the MQW sample with respect to the input signal; the area of the hysteresis loop is reduced when the laser photon energy is in correspondence with the exciton peaks [Figs. 9(c) and 9(e)], whereas in the case of photon energy intermediate between the excitons energy we have a good nonlinear response of the MQW waveguide [Fig. 9(d)], giving a curve well separated from the static characteristics; the cycles become larger and less regular if the laser pulse is positioned appropriately off resonance from the exciton peaks, with a tendency to follow the static curve. This is clear evidence of the different contributions of absorptive and dispersive effects; on resonance with the exciton peaks the first phenomenon is dominant, bistability is absent, and the hysteresis cycles are small and have a triangular shape, due to the strong absorption of the optical power in the initial part of the pulse and to the saturation of the carriers for the rest of the pulse, which travels almost unchanged across the waveguide. On the contrary, in Figs.

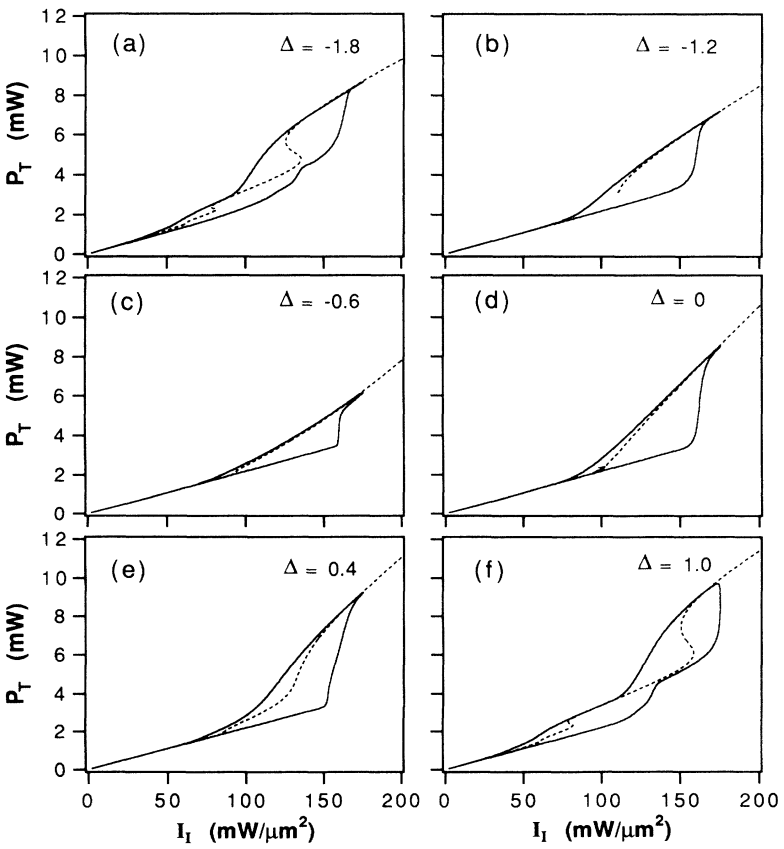

FIG. 9. Transmitted power P_T (in mW) vs incident intensity I_I (in mW/μm^2) for different values of the normalized detuning Δ (indicated in the graphs), calculated with the semiempirical optical response model, with $\delta=0$ and maximum incident intensity 180 mW/μm^2. Full line, dynamical curve; dashed line, static response.

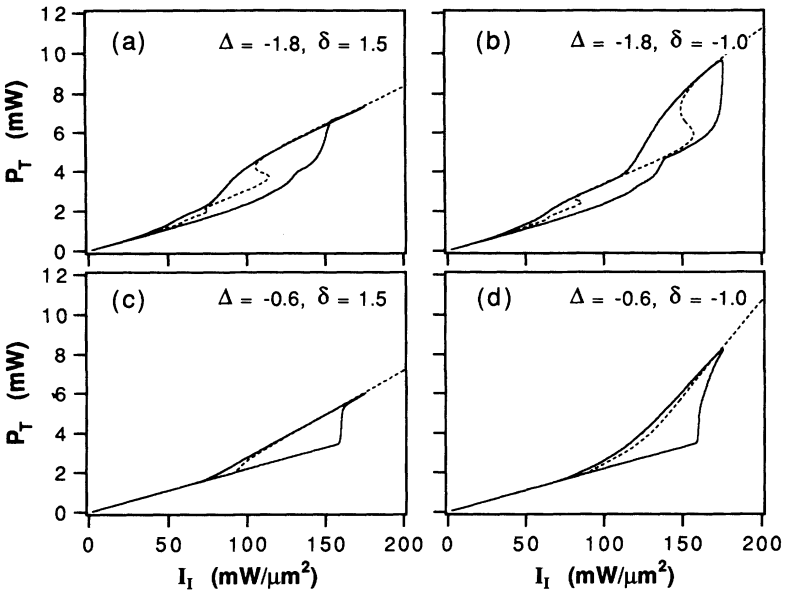

FIG. 10. Transmitted power P_T (in mW) vs incident intensity I_I (in mW/μm^2) for the cases of Figs. 9(a) and 9(c) with different values of the cavity detuning δ, as indicated in the graphs. Full line, dynamical curve; dashed line, static response.

9(a) and 9(f) the dispersion is dominant because, as one can see from Fig. 8, out of the exciton peaks the contribution of absorption is minor but the variations of refraction index are still sensible; multistability is observed, and the hysteresis loops have a complex shape due to cavity resonance phenomena; the same behavior was observed in the experimental curves (Fig. 4).

Another observation which confirms this interpretation is shown in Fig. 10, where we have plotted curves obtained with the same parameters of Figs. 9(a) and 9(c), but with a different value for the cavity detuning δ; this parameter is not easily controllable from an experimental point of view, and therefore it is a free parameter in our numerical simulation. It is possible to note that, in the case of a dispersion-dominated phenomenon [$\Delta=-1.8$, Figs. 10(a) and 10(b)], by varying the cavity detuning δ, there is a modification of the shape of the static curves for high incident intensity and a noteworthy variation of the hysteresis cycle, due to the shift of the cavity resonances, whereas in the case of dominant absorption [$\Delta=-0.6$, Figs. 10(c) and 10(d)] the variation is less evident.

It is important to study the minimum pulse peak intensity necessary to observe hysteretic behavior, also in the absence of bistability, to compare with the experimental observations (Sec. IV). Setting the photon energy between the two exciton peaks, (i.e., $\Delta=0$) and varying I_M, the maximum input laser intensity reached during the Gaussian optical pulse, we have obtained the results shown in Fig. 11. In particular, in Fig. 11(a) the intensity I_M of the optical pulse is too low and the response of the MQW waveguide is perfectly linear, while in Fig. 11(b) the intensity is above threshold, coincident with the change in slope of the static curve, and the hysteresis ap-

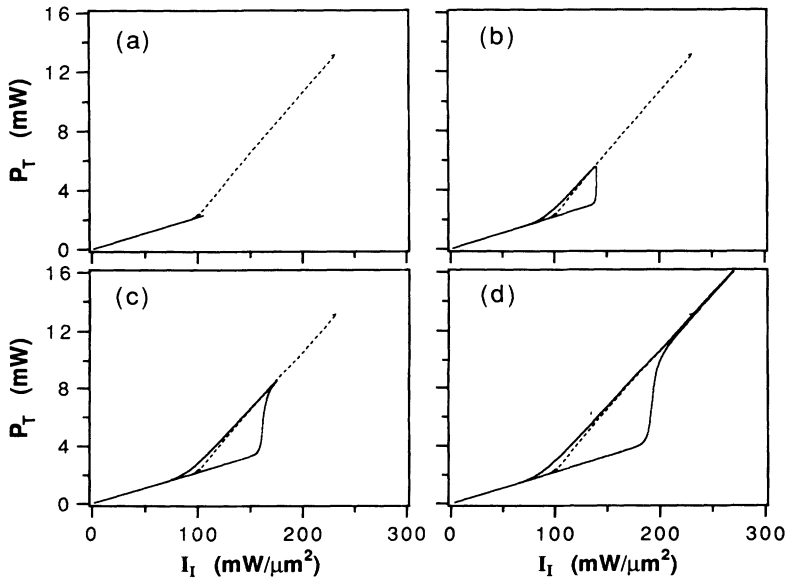

FIG. 11. Transmitted power P_T (in mW) vs incident intensity I_I (in mW/μm^2) obtained by varying the maximum height of the optical pulse, for the same parameters as Fig. 9(d); (a) $I_M=100$ mW/μm^2; (b) $I_M=140$ mW/μm^2; (c) $I_M=170$ mW/μm^2; (d) $I_M=280$ mW/μm^2. Full line, dynamical curve; dashed line, static response.

pears; well above the threshold [Figs. 11(c) and 11(d)] we also have a saturation phenomenon which makes the system jump to the high transmission branch well before I_I has reached its maximum value I_M.

Finally in Fig. 12 we plot some hystersis cycles calculated with the same parameters as in Fig. 9, but using the complete first-principles model for the optical response of the MQW waveguide (Fig. 7) discussed in Sec. V A. To obtain a nonlinear behavior in the complete model, it is necessary that the input laser pulse have a maximum intensity I_M larger than in the semiempirical model, especially if the photon energy is above the first exciton peak, because the presence of free-carrier recombination induces a strong absorption; this is particularly evident in Fig. 12(d), in which the hysteresis cycle disappears completely; as one can see from the static response, the nonlinear part of the curve shifts to high values of the incident intensity, and becomes less and less pronounced. The cycle can manifest itself only by increasing the intensity of the optical pulse well over the value used in the previous cases where we used the semiempirical model for optical response, an optical pulse with maximum intensity $I_M = 180$ mW/μm^2, and in which the hysteresis cycle persists. In Figs. 12(a)–12(c) it is possible to observe the same phenomenology already discussed, although with a reduced area of the hysteresis cycles; in the case of laser photon energy detuned from resonance with the exciton peak [Fig. 12(a)] there is a multistability phenomenon. Both the comparison between the numerical and experimental results for the hysteresis cycles and the anomalous behavior of the observed photoluminescence can be explained by the hypothesis, made at the end of Sec. III, that recombination in the MQW ridged waveguides takes place through diffusion to the ridge walls and nonradiative processes.

VII. CONCLUSIONS

This paper has reported the experimental observation of hysteretic behavior in a GaAs/$Al_xGa_{1-x}As$ MQW device, based on a ridged waveguide and under conditions quite different from those which characterize the previous experimental observations of optical bistability in MQW. The main reasons for exploring the present experimental arrangement of planar waveguide configuration lie in the determination of a MQW configuration more appropriate for practical optically bistable devices. Furthermore, the ridged waveguide configuration represents an intermediate step towards the use of quantum wire and quantum dot structures that present large optical nonlinearities, which are of interest for the realization of optically bistable devices.

The main aim of low bistability threshold with planar waveguides, which was pointed out by some of us in a previous publication [17], has not been achieved in the reported experimental observation. This is ascribed to technological difficulties in realizing a sample with a low threshold bistability; a sample shorter than the one we used and with low-transmission Bragg reflectors at the ends should be used. Thus the joint effort of experimental and theoretical investigation has been directed towards the test of optical hysteresis in the MQW planar waveguide configuration and the precise theoretical modeling. In effect, the numerical simulations turn out to be in satisfactory qualitative and semiquantitative agreement with the experimental data.

The results presented for the optical nonlinearities observed in the ridged waveguides are not affected by thermal effects. Thermal nonlinearities, due in particular to the heat generated by the nonradiative recombination of carriers, could play an important role in experiments on nonlinear transmission of semiconductors. The thermal response of the sample and the consequent optical nonlinearity takes place in the scale of the thermal conduction time [3]. This time depends principally on the temperature and geometry of the sample, and in our case it can be estimated as a few microseconds. The results for the optical nonlinearity presented in this work correspond to a time scale of 10 ns, when thermal non-

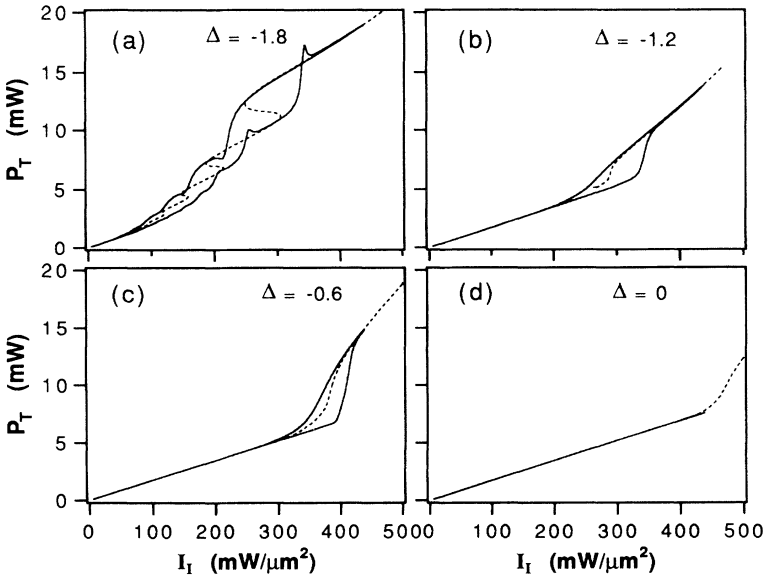

FIG. 12. Transmitted power P_T (in mW) vs incident intensity I_I (in mW/μm^2) for different values of normalized detuning Δ (indicated in the graphs), calculated with the first-principles model for optical response (Sec. V A); the maximum incident intensity of the pulse is $I_M = 440$ mW/μm^2. Full line, dynamical curve; dashed line, static response.

linearities are not yet developed. We have verified experimentally that thermal effects are not significant in our experimental conditions by observing the optical nonlinearities of ridged waveguides with different dimensions. The optical transmission was not affected significantly by the waveguide dimensions, while the thermal nonlinearities should depend on the heat conduction and sample dimensions.

According to our calculations, the MQW waveguide clearly displays an optical multistability when the photon energy of the incident laser is detuned with respect to the exciton peaks, due to the predominance of a dispersive nonlinearity; on the contrary, when the photon energy is in correspondence with the peaks, the nonlinearity is less relevant and steady-state bistability is absent. The experimentally observed hysteresis is dynamically induced [36] by the temporal variation of the input intensity in combination with the nonlinear response of the system. This hysteresis cycle has a very regular shape when the incident laser is tuned to the exciton peaks; otherwise, it has a complicated shape, due to the underlying multistability.

As a matter of fact, in the experiment it is not possible to decrease arbitrarily the rate at which the input intensity is swept forward and backward over the hysteresis cycle; on the contrary, in the numerical simulation the sweep rate of the intensity can be arbitrarily varied. The result of the simulations at different sweep rates is that, when the sweeping rate is reduced up to two orders of magnitude with respect to that applied in the experiment, the curve of the output power as a function of the input power strongly resembles the standard hysteresis cycle of static OB, or it is reduced to the nonlinear characteristics of the MQW waveguide if no steady-state bistability is there, as in the case of Figs. 9(c)–9(e). Another observation is that usually the dynamical sweeping produces a smoothing of the underlying steady-state cycle, which becomes more pronounced upon increase of the sweeping rate. All these calculations indicate the possibility to observe static OB in a MQW waveguide, using a suitable setup; furthermore, dynamical behavior can be further explored in more extended numerical simulations and, hopefully, in experiments with cw lasers, whose intensity can be ramped up and down at arbitrary rates.

ACKNOWLEDGMENTS

This research has been partially supported through Progetto Finalizzato Telecomunicazioni of the CNR, Italy. The MQW samples have been provided by Y. Chen and F. Bassani of the Scuola Normale Superiore in Pisa. The chemical etching has been performed by A. Stano at the CSELT Laboratories in Torino. The authors are grateful to F. Bassani, Y. Chen, M. Colocci, M. Cocito, R. Atanasov, F. Tassone, and A. Tredicucci for illuminating discussions and suggestions.

[1] E. Abraham and S. D. Smith, Rep. Prog. Phys. **45**, 815 (1982).
[2] L. A. Lugiato, *Theory of Optical Bistability,* in *Progress in Optics,* edited by E. Wolf (North-Holland, Amsterdam, 1984), Vol. XXI, p. 69.
[3] H. M. Gibbs, *Optical Bistability: Controlling Light with Light* (Academic, New York, 1985).
[4] H. M. Gibbs, S. L. McCall, T. N. C. Venkatesan, A. C. Gossard, A. Panner, and W. Wiegmann, Appl. Phys. Lett. **35**, 451 (1981).
[5] D. A. B. Miller, C. T. Seaton, M. F. Prise, and S. D. Smith, Phys. Rev. Lett. **47**, 197 (1981).
[6] D. S. Chemla, D. A. B. Miller, P. W. Smith, A. C. Gossard, and W. Wiegmann, IEEE J. Quantum Electron. **QE-20**, 265 (1984).
[7] D. S. Chemla and D. A. B. Miller, J. Opt. Soc. Am. B **2**, 1155 (1985).
[8] O. Sohler, U. Olin, E. Masseboeuf, G. Landgren, and M. Rask, Appl. Phys. Lett. **50**, 1559 (1987).
[9] R. Kuszelewicz, J. L. Oudar, J. C. Michel, and R. Azoulay, Appl. Phys. Lett. **53**, 2138 (1988).
[10] B. Sfez, J. L. Oudar, J. C. Michel, R. Kuszelewicz, and R. Azoulay, Appl. Phys. Lett. **57**, 324 (1990).
[11] S. W. Koch, N. Peyghambarian, and H. M. Gibbs, J. Appl. Phys. **63**, 21 (1988).
[12] S. H. Park, J. F. Morhange, A. D. Jeffrey, R. A. Morgan, A. Chavez-Pinson, H. M. Gibbs, S. W. Koch, N. Peyghambarian, M. Derstine, A. C. Gossard, J. H. English, and W. Wiegmann, Appl. Phys. Lett. **52**, 1201 (1988).
[13] B. Sfez, J. L. Oudar, J. C. Michel, R. Kuszelewicz, and R. Azoulay, Appl. Phys. Lett. **57**, 1849 (1990).
[14] J. L. Oudar, B. Sfez, R. Kuszelewicz, J. C. Michel, and R. Azoulay, Phys. Status Solidi B **159**, 181 (1990).
[15] B. Sfez, R. Kuszelewicz, and J. L. Oudar, Opt. Lett. **16**, 855 (1991).
[16] J. E. Ehrlich, D. T. Nelson, A. C. Walker, G. T. Kennedy, R. S. Grant, W. Sibbett, M. Hopkinson, and M. Pate, Appl. Phys. Lett. **63**, 1610 (1993).
[17] G. P. Bava, F. Castelli, P. Debernardi, and L. A. Lugiato, Phys. Rev. A **45**, 5180 (1992).
[18] H. Haug and S. Schmitt-Rink, J. Opt. Soc. Am. B **2**, 1135 (1985).
[19] S. Schmitt-Rink and C. Ell, J. Lumin. **30**, 585 (1985).
[20] S. Schmitt-Rink, C. Ell, and H. Haug, Phys. Rev. B **33**, 1183 (1986).
[21] H. Haug and S. W. Koch, Phys. Rev. A **39**, 1887 (1989).
[22] C. Ell, R. Blank, S. Benner, and H. Haug, J. Opt. Soc. Am. B **6**, 2006 (1989).
[23] H. Haug and S. W. Koch, *Quantum Theory of the Optical and Electronic Properties of Semiconductors* (World Scientific, Singapore, 1990).
[24] G. P. Bava and P. Debernardi, Electron. Lett. **27**, 603 (1991).
[25] Y. Chen, R. Cingolani, J. Massies, G. Neu, F. Turco, and J. C. Garcia, Nuovo Cimento **10**, 1093 (1988).
[26] Y. Chen, R. Cingolani, L. C. Andreani, F. Bassani, and J. Massies, Nuovo Cimento **10**, 847 (1988).
[27] A. Stano, J. Electrochem. Soc. **134**, 448 (1987).
[28] M. Shinada and S. Sugano, J. Phys. Soc. Jpn. **21**, 1936

(1966).
[29] M. Colocci, M. Gurioli, A. Vinattieri, F. Fermi, C. Deparis, J. Massies, and G. Neu, Europhys. Lett. **12**, 417 (1990).
[30] N. Peyghambarian and H. M. Gibbs, J. Opt. Soc. Am. B **2**, 1215 (1985).
[31] P. Debernardi, A. Pisoni, and G. P. Bava, J. Quantum Electron. (to be published).
[32] G. P. Bava and L. A. Lugiato, Opt. Commun. **78**, 195 (1990).
[33] D. Marcuse, *Theory of Dielectric Optical Waveguide* (Academic, New York, 1974).
[34] H. Risken and K. Nummedal, J. Appl. Phys. **39**, 4662 (1968).
[35] H. Haken, *Synergetics—An Introduction* (Springer, Berlin, 1974).
[36] T. Erneux and P. Mandel, Phys. Rev. A **28**, 896 (1983); P. Mandel and T. Erneux, Phys. Rev. Lett. **53**, 1818 (1984).